Available Online

J. Sci. Res. **17** (1), 165-176 (2025)

JOURNAL OF SCIENTIFIC RESEARCH

www.banglajol.info/index.php/JSR

Comparative study of Pure and D-Malic Acid Doped Potassium Boro Oxalate Crystal: Special Attention on the Structural, Optical, Thermal, and Nonlinear Optical Properties

S. D. Yadav[1,2], M. I. Baig[2*], M. Anis[3]

[1]Department of Physics, Yashwantrao Chavan College of Science Karad, Vidyanagar, Karad, 415124, Maharashtra, India

[2]Department of Physics, Prof. Ram Meghe College of Engineering and Management, Badnera, Amravati, 444701, Maharashtra, India

[3]Department of Physics and Electronics, Maulana Azad College of Arts, Science and Commerce, Dr. Rafiq Zakaria Campus I, Chhatrapati Sambhajinagar, 431001, Maharashtra, India

Received 29 June 2024, accepted in final revised form 30 September 2024

Abstract

Single crystals of potassium boro oxalate (KBO) and D-malic acid doped KBO (DMA-KBO) were grown by the slow evaporation method at room temperature. The crystal structure has been confirmed by the single-crystal X-ray diffraction method. The understudied material's functional groups have been confirmed by Fourier Transform Infrared spectroscopy (FT-IR). Their optical parameters have been evaluated using UV-visible (UV-Vis) spectroscopy. UV-Vis spectroscopy revealed higher transmittance in the visible region, with band gap energies reported at 5.35 eV for pure KBO crystals and 5.65 eV for those doped with malic acid. Scanning electron microscopy (SEM) analysis explores the structural morphology of the grown crystal. Energy dispersive X-ray spectrometry (EDS) has been employed to validate the effective incorporation of malic acid. Thermogravimetric and differential thermal analysis (TGA/DTA) revealed that the doped crystals exhibited thermal superiority over the pure KBO. Laser damage analysis showed that doping enhanced the crystals' resistance to laser radiation.

Keywords: Crystal Growth; SEM-EDS analysis; Optical Constants; Laser damage threshold.

doi: https://dx.doi.org/10.3329/jsr.v17i1.74520 J. Sci. Res. **17** (1), 165-176 (2025)

1. Introduction

The photonic industry is in quest of crystals that exhibit good linear and nonlinear properties. Crystal with exceptional linear and nonlinear properties utilize as component in devices involved in the domain of frequency conversions, data storage, optical switching, etc. [1-4]. In the current scenario, Researcher gives much attention to semi-organic compounds owing to the wide transparency window, efficient second harmonic generation, thermal stability, significant nonlinearity, high resistance to laser damage, and strong

* *Corresponding author*: mirza.baig@prmceam.ac.in

mechanical hardness. Such outstanding traits of semi-organic materials enable technocrats for utilization of crystals for device fabrication [5-7].

Borate-based metal-organic compounds have unique nonlinear properties, attributed to anionic groups like BO_4 and BO_3. Moreover, the incorporation of π-conjugated planar groups from organic material enhances birefringence, while the synergy between anionic groups and metal cations amplifies the Second Harmonic Generation. Recently, materials from the metal-organic borate family, including potassium boro succinate, potassium boro oxalate (KBO), potassium boro dicitrate, and Boric acid potassium acetate have been synthesized and studied [8-11]. Among variously reported borate crystals, Potassium Boro Oxalate is an exciting nonlinear optical (NLO) crystal owing to structural, optical, electrical, second harmonic generation (SHG) efficiency, photoconductivity, and thermal behavior [10,12,13]. Several researchers adopted different ways to optimize KBO material but among all, Literature review hints that doping is more reliable and convenient in optimizing the KBO material. Maleic acid (MA), possesses a strong net dipole moment and hence could play a crucial role in enhancing the optical, thermal, and dielectric performance, mechanical strength, and overall characteristics of the host material [14,15]. In literature, Doping crystals with 1 mol% DL-malic acid considerably improves crystals' growth, Mechanical and linear and nonlinear properties of Potassium dihydrogen phosphate (KDP) and ammonium dihydrogen phosphate (ADP) crystal [16,17]. L-malic acid sodium nitrate has improved mechanical properties and thermal stability. It exhibits 0.8 times the SHG efficiency of KDP, making it appropriate for optical applications. Combining L-alanine and DL-malic acid improves mechanical strength and optical properties. It shows equivalent SHG properties compared with KDP, which is useful for nonlinear optical (NLO) and electro-optic devices. DL-malic acid-doped zinc tris (thiourea) sulfate (ZTS) crystals exhibit improvement of wide transmittance range, thermal stability, and 1.55 times the SHG efficiency of KDP, making them suitable for nonlinear optical systems. These findings show the potential of malic acid doping to improve NLO and optical characteristics in photonic devices [18-21]. Recently, the optical properties of KBO have been enhanced through the introduction of L-valine doping [22].

Hitherto, as per the literature review, doping malic acid into KBO has yet to be reported by any researcher, making this investigation novel. Also, the merits of malic acid promote our research group to doped malic acid into KBO crystal. The current research doping of 1 mol malic acid into host KBO material. Subsequently, optical, thermal, and mechanical properties the impact of malic acid on the structural, optical, thermal, and mechanical properties of KBO crystal has been investigated, and results discussed.

2. Experimental Details

2.1. *Material synthesis*

Potassium boro oxalate (KBO) single crystals have been grown using the slow evaporation solution growth approach. A high-purity potassium hydroxide, boric acid, and oxalic acid

(Merck Grade, Germany) solution in a 1:1:1 ratio with deionized water was stirred constantly at 40 °C for 8 h until it became clear and homogenous. The saturated solution was purified and let to evaporate in a controlled atmosphere. To improve purity, the material was recrystallized repeatedly. Spontaneous nucleation produced tiny, translucent seed crystals. A defect-free seed crystal was chosen and put in the mother solution, which was kept at a constant 34 °C. Over 17 days, crystals with an average size of 6 x 4 x 2 mm^3 were grown. To synthesize DMA-KBO, 1 mol of malic acid was added to the prepared KBO solution. The growth parameters for DMA-KBO were maintained the same as for pure KBO. Transparent, high-quality DMA-KBO crystals started to form within 5 days, and a well-grown crystal measuring 20 x 10 x 4 mm^3 was harvested within 14 days. Figs. 1 (a) and 1 (b) illustrate the as-grown single crystal of pure KBO and DMA-KBO.

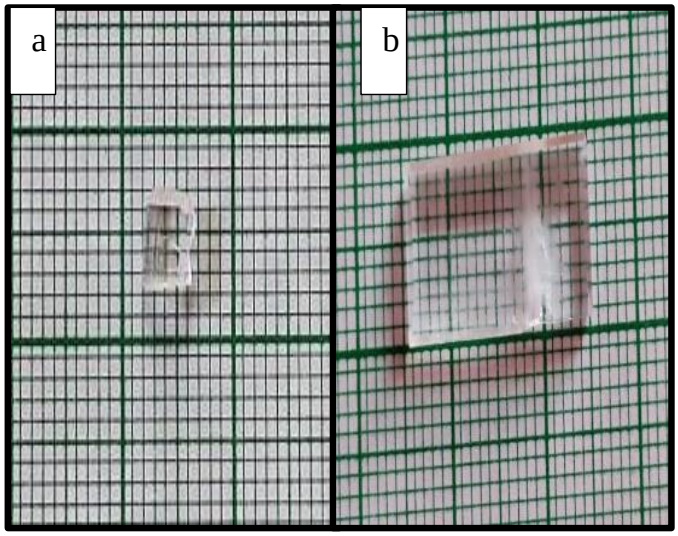

Fig. 1. Grown single crystal of a) Pure KBO and b) DMA-KBO.

3. Results and Discussion

3.1. *Single crystal XRD*

Single crystal x-ray diffraction (SXRD) analysis was conducted to determine the cell parameters and structure of pure KBO and DMA-KBO crystals using an ENRAF NONIUS CAD 4 automatic XRD. The results showed that pure KBO and DMA-KBO crystals have an orthorhombic structure with a $P2_12_12_1$ space group. The details of SXRD data are summarised in Table 1. The SXRD results revealed that pure KBO crystal parameters closely match previously reported values [10,23]. The presence of malic acid might have induced strain in the lattice causing minor changes in the lattice parameters and volume of DMA-KBO.

Table 1. Comparison of SXRD data for pure KBO and DMA-KBO.

Crystal data	KBO (Reported) [10,23]	KBO (Present work)	DMA-KBO (Present work)
a (Å)	3.726	3.772	3.783
b (Å)	9.503	9.572	9.586
c (Å)	17.772	17.833	17.941
α	90°	90°	90°
β	90°	90°	90°
γ	90°	90°	90°
Volume (Å^3)	629.27	643.870	650.609
System	Orthorhombic	Orthorhombic	Orthorhombic
Space group	$P2_12_12_1$	$P2_12_12_1$	$P2_12_12_1$

3.2. *FT-IR spectral analysis*

The FTIR spectrum of KBO and DMA-KBO crystals revealed characteristic vibrational frequencies corresponding to various functional groups present in the compound which are shown in Fig. 2. The observed peaks at 3292 cm^{-1} and 3160 cm^{-1} indicate O-H stretching vibrations, indicative of hydroxyl groups. A prominent peak at 1690 cm^{-1} corresponds to C=O stretching vibrations, attributed to carbonyl groups originating from oxalic acid. The presence of boron-oxygen bonds is evidenced by peaks at 1380 cm^{-1} and 815 cm^{-1}, corresponding to B-O asymmetric and symmetric stretching vibrations, respectively, arising from boric acid. Additionally, the presence of hydroxyl groups is further supported by the O-H bending vibration observed at 655 cm^{-1}. The FTIR spectral features collectively confirm the expected functional groups in KBO. FTIR peaks corresponding to the functional groups are in close agreement with the existing literature [10,12,13]. The variations in peak intensities and shifts in peak positions in the doped KBO single crystal may be due to the presence of hydroxyl and carbonyl groups in malic acid thus confirming the incorporation of malic acid.

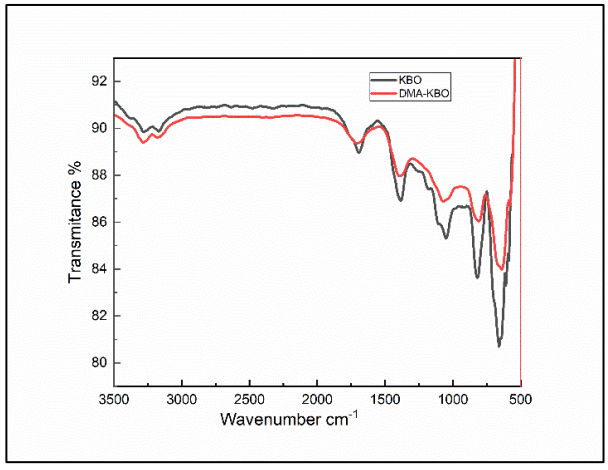

Fig. 2. FTIR spectrum of pure KBO and DMA-KBO.

3.3. *SEM and EDS analyses*

The single crystals of KBO and DMA-KBO were examined using a JEOL JSM-IT200 Scanning electron microscope (SEM) with an accelerating voltage range of 0.5 to 20 kV. The SEM images and EDS analysis of pure KBO and DMA-KBO crystals are shown in Figs. 3 and 4. for pure KBO and DMA-KBO respectively. SEM picture of pure KBO and DMA-KBO crystals shows the same kind of morphology with irregularly formed particles with big, flat plates and tiny pieces, suggesting high crystallinity and brittleness. There is no inclusive change in the morphology of DMA-KBO.

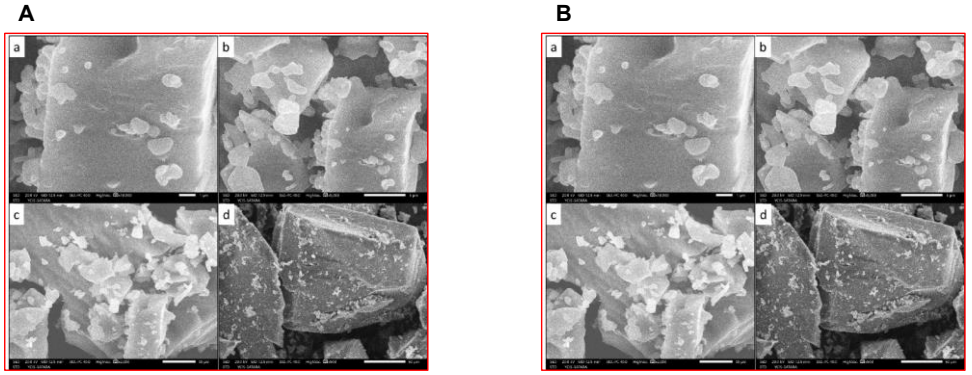

Fig. 3. SEM images of (A) pure KBO and (B) DMA-KBO at (a) 1 µm, (b) 5 µm, (c)10 µm and (d) 50 µm magnifications.

The EDS examination of pure KBO found 22.21 % carbon, 62.70 % oxygen, and 15.09 % potassium by mass. SEM pictures of DMA-KBO crystals revealed more varied forms and a granular flat surface texture, indicating enhanced catalytic capabilities. These crystals showed a greater connection between particles, which improved mechanical stability. The EDS examination of DMA-KBO revealed 35.76 % carbon, 52.58 % oxygen, and 11.66 % potassium by mass indicating the incorporation of MA in KBO. The different particle shapes and granular texture increase surface area, which enhances catalytic properties. Improved particle connection leads to a more robust structure, which is useful for applications that need great mechanical stability such as microhardness and resistance to laser damage.

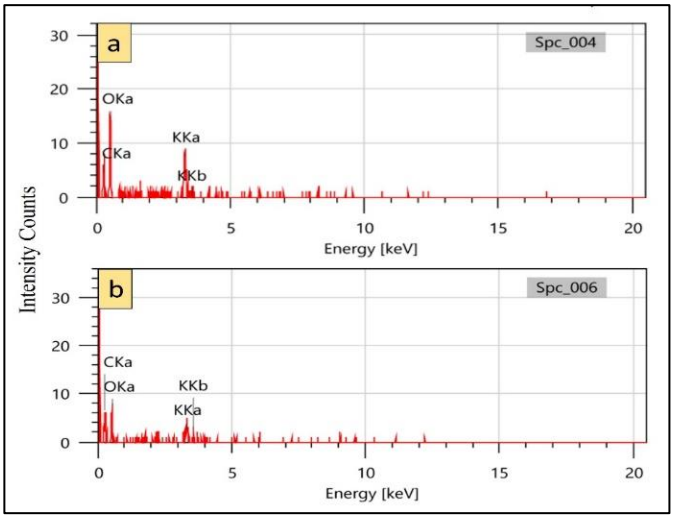

Fig. 4. EDS spectra for a) pure KBO and b) DMA-KBO.

3.4. *UV VIS spectral analysis*

The optical absorption spectra of KBO and DMA-KBO single crystals were recorded using a Systronics Double Beam UV-Vis Spectrophotometer 2202. The absorption and transmittance percentages for KBO and DMA-KBO as a function of wavelength are illustrated in Fig. 5.

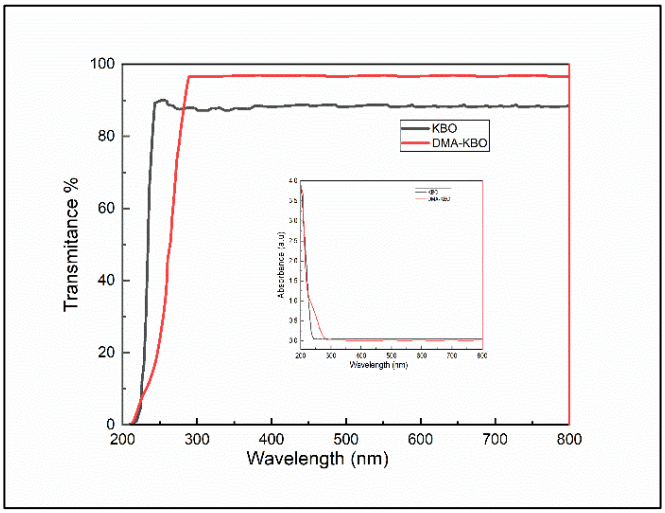

Fig. 5. Comparison of optical spectra for pure KBO and DMA-KBO.

The transmittance graph shows that KBO and DMA-KBO crystals have a wide transmission window above 240 nm, which matches earlier reports [12,23]. Pure KBO exhibited 86 % transmittance, while DMA-KBO showed 97%, which shows a 19% hike in transmittance compared to KDP crystal [17]. Due to carboxylic acid functional groups present in malic acid, form extensive networks of bonds. These networks facilitate the delocalization of π-electrons, which enhances electronic properties such as conductivity and optical transparency. This π-electron delocalization benefits materials science applications, strengthening doped crystals' structural and optical properties. These improvements make the materials suitable for optical and optoelectronic device applications [24]. The UV absorption edge for KBO was detected around 250 nm, with a lower cutoff wavelength of 248 nm for pure KBO and 296 nm for DMA-KBO, as confirmed by the absorbance graph. The relationship between the optical absorption coefficient and photon energy is valuable for examining the band structure and types of electron transitions. The optical absorption coefficient (α) was determined using the equation derived from the transmittance data [25].

$$\alpha = (2.303\ log\ (1/T))/d \quad (1)$$

where T is the transmittance and d is the thickness of the crystal. The grown crystals of thickness 3 mm were used to determine the optical absorption coefficient (α) from transmittance measurements for both pure and malic acid-doped KBO. As a direct band gap material, the crystal under study has a specific type of electronic band structure. In this structure, electrons can make a direct transition between energy levels. For high photon energies (hν), the absorption coefficient (α) of the crystal follows a particular mathematical relationship. This relationship describes how efficiently the crystal absorbs light at different photon energies.

$$(\alpha h\nu)^2 = A(h\nu - E_g) \quad (2)$$

where α is the absorption coefficient, E_g is the band gap and A is the constant. To determine the energy bandgap, a Tauc's plot was used, Fig. 6 shows plotting photon energy (hν) versus $(\alpha h\nu)^2$ for pure KBO and DMA-KBO respectively.

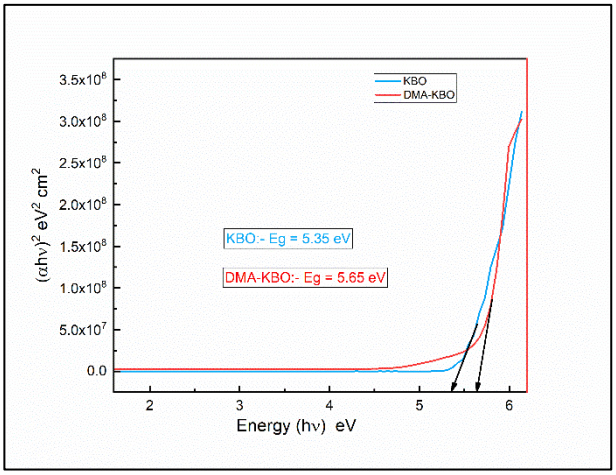

Fig. 6. Plot of (hν) versus $(\alpha h\nu)^2$ for pure KBO and DMA-KBO.

The optical bandgap was calculated by extrapolating the linear portion of the graph to the x-axis. The band gap was found to be 5.35 eV for KBO, which is in good agreement with reported values of the band gaps for pure KBO (5.30 ev) [12] and for DMA-KBO (5.65 eV). A larger band gap correlates with better transparency in the visible spectrum because photons with energy less than the band gap i.e. visible light photons are not absorbed by the material. These results indicate good transparency and potential for nonlinear optical applications.

The increased band gap from 5.35 eV to 5.65 eV indicates that the DMA-KBO absorbs less visible light than the undoped KBO, thus enhancing its transparency. This significant bandgap suggests that the developed crystals possess dielectric properties, allowing them to polarize under intense radiation. The absorption spectrum analysis showed a lower cutoff wavelength of 250 nm, indicating minimal absorption and effective transmission of laser beams within the 250 nm to 800 nm range. This demonstrates the crystal's excellent transparency across the UV-visible and near-IR regions, making it ideal for nonlinear optical (NLO) applications [25,26].

3.5. *Determination of optical constants*

The manufacturing procedure influences a crystal's optical characteristics. Key features like the extinction coefficient influence how light interacts with the material. The extinction coefficient (K) is essential and plays an important role in determining the optical constants of crystalline materials [18,26]. It measures the absorption of incident photon energy as it passes through the crystal. The extinction coefficient can be computed using the following equation:

$$\mathbf{K = \lambda\alpha/4\pi} \tag{3}$$

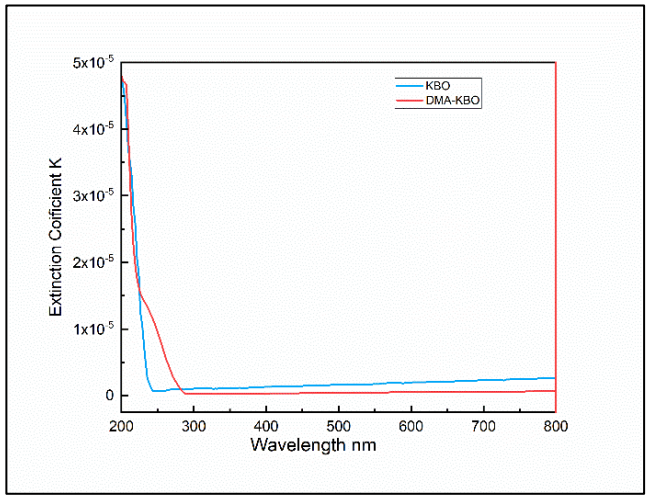

Fig. 7. Variation of extinction coefficient w.r.t. wavelength for pure KBO and DMA-KBO.

Fig. 7 depicts the extinction coefficient at various wavelengths for pure KBO and DMA-KBO. The trend observed in both graphs reveals that up to 250 nm for pure KBO and 280 nm for DMA-KBO respectively, the extinction coefficient has higher values while as the incident wavelength increases, the extinction coefficient decreases suddenly, and it remains relatively constant across the entire visible region. For pure KBO, at incident wavelength 532 nm, the extinction coefficient is 1.86 x 10^{-6}; DMA-KBO has 0.424 x 10^{-6}, which shows less absorption. At the UV region, the higher extinction coefficient indicates strong absorption due to electronic transitions. In KBO crystals, these transitions are typically associated with the absorption of photons that promote electrons to higher energy states. When malic acid is added to KBO, it introduces new energy levels or states within the crystal structure. As the incident wavelength increases, the photons have less energy, which might not be sufficient to promote electronic transitions, resulting in decreased absorption. This is why the extinction coefficient drops suddenly and then stabilizes. In the visible region, both pure KBO and DMA-KBO show relatively constant and low extinction coefficients, indicating that they are transparent to visible light. This transparency is essential for applications in optics and photonics where minimal absorption in the visible range is desired. The extinction coefficient at 532 nm for pure KBO is 1.86 x 10^{-6}, whereas for DMA-KBO, it is 0.424 x 10^{-6}. The lower extinction coefficient for DMA-KBO at this wavelength indicates slightly higher transmittance. Transparency is inversely related to the extinction coefficient higher K means lower transparency, and lower K means higher transparency. This inverse relationship explains why materials with low extinction coefficients are used in applications where high transparency is required. These new states can interact with the UV light differently, shifting the absorption peak slightly indicating that DMA alters the electronic environment of KBO. This trend underscores the preference for materials with low extinction coefficients in the visible and near-infrared spectrums, particularly in optical components such as lenses, windows, and fibers. Such materials facilitate efficient light transmission by minimizing absorption and optimizing performance [25,27].

3.6. *Thermal analysis*

Thermogravimetric analysis (TGA) and differential thermal analysis (DTA) were carried out on KBO crystals and DMA-KBO crystals. These analyses were conducted using a thermal analyzer at a 20 °C/min heating rate, ranging from 50 °C to 600 °C in a nitrogen atmosphere. The DGA/DTA and TG curves for KBO and DMA-KBO crystals are presented in Fig. 8, respectively. Fig. 8(a) shows that the KBO crystal remains thermally stable up to 220 °C, with a second endothermic peak at 220 °C indicating its melting point. DTG curves show that decomposition starts at 280.2 °C, marked by a significant weight loss. This decomposition is associated with the release of oxides of boron and potassium, indicated by exothermic peaks at 250.2 °C and 530.8 °C. From the TG curve, it is observed that up to 100 °C there is significant weight loss i.e., up to 23 %. From 100 °C to 250 °C there is approximately 9 % weight loss observed, and from 250 °C to 350 °C it is seen that there is

significant weight loss up to 18 %. The sharpness of these peaks suggests a high level of crystallinity and purity in the sample.

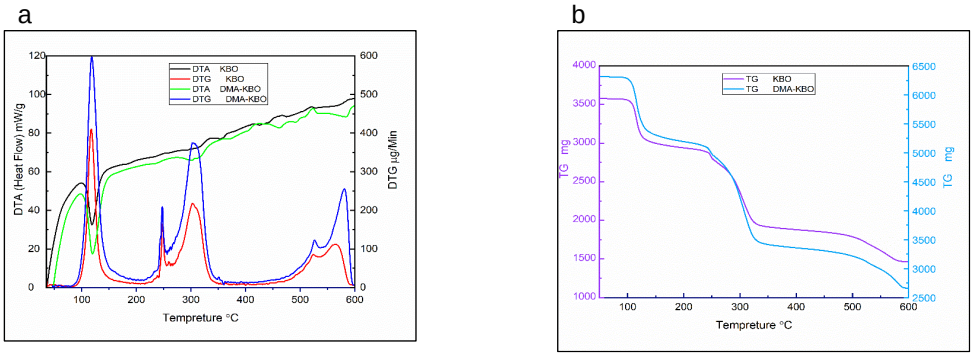

Fig. 8. (a) DTA / DTG and (b) TGA / DTA curves for pure KBO and DMA-KBO.

The graphs show that the KBO crystal doped with malic acid is stable up to 100 °C. The initial endothermic peak at 100 °C in the DTA curve likely corresponds to the release of water molecules. The doped sample shows another endothermic peak around 235 °C, indicating its melting point. Similar to the undoped sample, significant decomposition starts at approximately 300 °C. The doped sample exhibits further decomposition events around 500 °C, as suggested by exothermic peaks in the DTA curve and corresponding peaks in the DTG curve at 100 °C, 300 °C, and 500 °C, which indicate the rates of weight loss. From the TG curve, Fig. 8b, it is observed that up to 100 °C there is significant weight loss i.e. up to 14 %. From 200 °C to 350 °C there is approximately 32 % weight loss observed, and from 350 °C to 600 °C it is seen that there is gradual weight loss of up to 10 %. From the graphs, it looks like the KBO crystal remains thermally stable up to 220 °C, while the KBO crystal doped with malic acid shows little complex thermal behavior, with stability up to 235 °C and decomposition stages beyond 300 °C. In comparison, DMA-KBO is more thermally stable than pure KBO. These differences are important for applications requiring specific thermal stability.

3.7. *Laser damage analysis*

To the best of our knowledge, this is the first time the laser damage threshold of pure and malic acid-doped KBO crystals has been characterized. Both types of crystals, each 3 mm thick, were tested using a Q-switched Nd laser (QUANTA RAY LAB-170-10) with a wavelength of 1064 nm, a pulse width of 6 ns, and a repetition rate of 10 Hz. The laser beam was focused using a biconvex lens with a 10 cm focal length. For pure KBO crystals, visible damage, such as surface pitting and micro-cracks, was observed at an energy level of 12.5 mJ, marking the threshold where the crystal begins to deteriorate. In contrast, the DMA-KBO crystals showed damage at a higher energy level of 16.9 mJ, indicating significantly improved resistance. This increase in the damage threshold suggests that the doped crystals

have a stronger structure and are more suitable for high-power laser applications in demanding optical environments.

4. Conclusion

The slow evaporation method is utilized in harvesting good quality transparent single crystals of DMA-KBO. SXRD study confirms material crystal structure to the orthorhombic crystal system. FTIR spectroscopy examined the chemical bonding, and SEM-EDAX analysis verified the elemental composition and surface features. TGA-DTA studies revealed thermal stability up to 220 °C for pure KBO and 235 °C for doped KBO. UV-Vis absorption spectra showed transparency of 86 % for pure KBO and up to 97 % for doped KBO. Impressive values of optical parameters and laser damage threshold reveal that the grown crystals are suitable for optical device applications.

References

1. M. Anis, M. Shkir, S. AlFaify, M. I. Baig, A. M. Alshehri, and H. Algarni, Mater. Chem. Phys. **246**, ID 122809 (2020). https://doi.org/10.1016/j.matchemphys.2020.122809
2. M. I. Baig, M. Anis, S. Kalainathan, B. Babu, and G. G. Muley, Mater. Technol. **32**, 560 (2017). https://doi.org/10.1080/10667857.2017.1321275
3. C. A. Rao, K. Shakampally, and K. V. R. Murthy, J. Sci. Res. **13**, 891 (2021). https://doi.org/10.3329/jsr.v13i3.53287
4. N. Mahalakshmi and M. Parthasarathy. J. Sci. Res. **16**, 449 (2024). https://doi.org/10.3329/jsr.v16i2.67430.
5. M. Suriya, M. Manimaran, B. M. Boaz, and K. S. Murugesan, J. Mater. Sci. Electron. **32**, 11393 (2021). https://doi.org/10.1007/s10854-021-05265-2
6. N. Indumathi, A. Hemalatha, E. Chinnasamy, A. Venkatesan, M. E. R. Saravanan, K. Deepa, P. Matheswaran, S. Senthil, K. Kaviyarasu, and R. Uthrakumar, In Mater. Today: Proc. **36**, 150 (2019). https://doi.org/10.1016/j.matpr.2020.02.669.
7. S. Masilamani, A. M. Musthafa, and P. Krishnamurthi, P. Arabian J. Chem. **10**, S3962 (2017). https://doi.org/10.1016/j.arabjc.2014.06.003
8. V. Chithambaram, S. J. Das, R. A. Nambi, and S. Krishnan, Opt. Laser Technol. **43**, 1229 (2011). https://doi.org/10.1016/j.optlastec.2011.03.014
9. C. Kayalvizhi, S. Anand, R. Durga, B. S. Ebinezer, R. S. Sundararajan, Heliyon **6**, ID e03133, (2020). https://doi.org/10.1016/j.heliyon.2019.e03133
10. S. Sagadevan, Optik (Stuttg) **127**, 5613 (2016). https://doi.org/10.1016/j.ijleo.2016.03.067
11. M. K. Dhatchaiyini, G. Rajasekar, and A. Bhaskaran, J. Mater. Sci. **54**, 9362 (2019). https://doi.org/10.1007/s10853-019-03542-4
12. S. Devi and D. Jananakumar, Chinese J. Phys. **68**, 339 (2020). https://doi.org/10.1016/j.cjph.2020.09.018
13. G. Pasupathi, K. Murugadoss, M. Senthilkumar, and C. Ramachandraraja, Optik (Stuttg) **125**, 3389 (2014). https://doi.org/10.1016/j.ijleo.2013.12.086
14. M. Lakshmipriya, R. E. Vizhi, and D. R. Babu, Optik (Stuttg) **126**, 4259 (2015). https://doi.org/10.1016/j.ijleo.2015.08.126.
15. R. O. Priakumari, S. G. S. Sheba, and M. Gunasekaran, J. Mol. Struct. **1102**, 63 (2015). https://doi.org/10.1016/j.molstruc.2015.08.043.
16. S. Arulmani, K. Deepa, N. Indumathi, M. Viktor, A. Raj, and S. Senthil, Mechanics, Mater. Sci. Eng. (2017). https://doi.org/10.2412/mmse.30.76.146
17. M. Anis, G. G. Muley, M. I. Baig, S. S. Hussaini, and M. D. Shirsat, Mater. Res. Innovations **21**, 439 (2017). https://doi.org/10.1080/14328917.2016.1265250

18. M. Anis, G. G. Muley, A. Hakeem, M. D. Shirsat, and S. S. Hussaini, Opt. Mater. (Amst) **46**, 517 (2015). https://doi.org/10.1016/j.optmat.2015.04.064
19. N. Saravanan, S. Santhanakrishnan, S. Suresh, S. S. J. Dhas, P. Jayaprakash, and V. Chithambaram, J. Mater. Sci.: Mater. Electron. **29**, 18449 (2018). https://doi.org/10.1007/s10854-018-9960-9
20. B. Sivasankari and P. Selvarajan, Optik (Stuttg) **127**, 4928 (2016). https://doi.org/10.1016/j.ijleo.2016.01.148
21. D. Jaikumar, S. Kalainathan, and G. Bhagavanarayana, J. Cryst. Growth **312**, 120 (2009). https://doi.org/10.1016/j.jcrysgro.2009.09.056
22. S. Devi and D. Jananakumar, Chinese J. Phys. **71**, 159 (2021). https://doi.org/10.1016/j.cjph.2020.09.025.
23. D. Jananakumar, P. Mani, D. Jananakumar, and P. Mani, Mater. Phys. Mech. **16**, 92 (2013).
24. P. Karuppasamy, M. S. Pandian, P. Ramasamy, and S. Verma, Opt. Mater. (Amst) **79**, 152 (2018). https://doi.org/10.1016/j.optmat.2018.03.041
25. R. Sangeetha, V. C. Vincent, G. Bakiyaraj, K. Kirubavathi, and K. Selvaraju, Results Optics **14**, ID 100607 (2024). https://doi.org/10.1016/j.rio.2024.100607
26. X. Chen and K. M. Ok, Chem Sci. **15**, 3942 (2022). https://doi.org/10.1039/d1sc07121a
27. V. R. Sagane, G. Vinitha, G. G. Muley, and P. M. Wankhade, Phys. Open **20**, ID 100224 (2024). https://doi.org/10.1016/j.physo.2024.100224